

# Generation of Transient Photocurrents in the Topological Surface State of $\text{Sb}_2\text{Te}_3$ by Direct Optical Excitation with Mid-Infrared Pulses

K. Kuroda,<sup>1</sup> J. Reimann,<sup>1</sup> J. Gdde,<sup>1</sup> and U. Hfer<sup>1</sup>

<sup>1</sup>*Fachbereich Physik und Zentrum fr Materialwissenschaften, Philipps-Universitt, 35032 Marburg, Germany*

(Dated: June 7, 2021)

We combine tunable mid-infrared (MIR) pump pulses with time- and angle-resolved two-photon photoemission to study ultrafast photoexcitation of the topological surface state (TSS) of  $\text{Sb}_2\text{Te}_3$ . It is revealed that MIR pulses permit a direct excitation of the unoccupied TSS owing to an optical coupling across the Dirac point. The novel optical coupling provokes asymmetric transient populations of the TSS at  $\pm k_{\parallel}$ , which mirrors a macroscopic photoexcited electric surface current. By observing the decay of the asymmetric population, we directly investigate the dynamics of the long-lived photocurrent in the time domain. Our discovery promises important advantages of photoexcitation by MIR pulses for spintronic applications.

PACS numbers: 73.20.-r, 78.47.J-, 79.60.-i, 79.60.Bm

Three-dimensional (3D) topological insulators (TIs) belong to a new class of materials which are characterized by an insulating bulk and a metallic topological surface state (TSS) [1]. The most remarkable properties of the TSS are its Dirac-cone-like energy dispersion and its chiral spin texture in  $k$ -space [2, 3]. The latter incorporates a protection against backscattering and is very promising for spintronic applications. Optical coupling to the chiral spin texture of TSSs offers many interesting phenomena, such as optical control of the spin [4], surface transport [5–7], and topological phases [8]. To exploit these exotic properties, a detailed understanding of the optical excitation and the subsequent electron dynamics are essential keys. A number of studies have investigated the ultrafast electron dynamics by optical methods like reflectivity [9], second harmonic generation [10], or by optically triggered detection of photocurrents [7]. These experiments, however, hardly show a pure photoexcitation of TSSs, since the bulk response typically governs the total signal.

Time- and angle-resolved two-photon photoemission (2PPE) is a particularly suited technique for this purpose [11], because it can directly image the optically excited electron population by energy-momentum mapping and makes it possible to follow the ultrafast carrier dynamics in the time domain by pump-probe schemes. This technique has been successfully applied for the study of the electron dynamics in 3D TIs [12–19] using pump laser pulses at 800-nm or in the visible range. In contrast to higher-lying states, such as image-potential states, however, the relevant TSS close to the Fermi energy ( $E_F$ ) is in these studies only indirectly excited by a delayed filling from states far above  $E_F$ . Under such conditions, a coherent optical control of the TSS population is difficult and its decay dynamics is masked.

In this Letter, we demonstrate that tunable low-energy pump pulses in the mid-infrared (MIR) regime are capable to induce a direct optical transition between the occupied and unoccupied part of the TSS across the Dirac

point (DP). We show this for the example of  $p$ -doped  $\text{Sb}_2\text{Te}_3$ , in which the most part of its Dirac cone is initially unoccupied [18, 19]. In contrast to a bulk mediated indirect population, this resonant TSS-TSS transition makes it possible to generate an asymmetry between the transient population of opposite parallel momenta  $k_{\parallel}$ , which directly mirrors a macroscopic spin polarized photocurrent within the TSS. By monitoring the decay of this asymmetry, we identify different scattering mechanisms of the electrons that carry the photocurrent.

Details of our optical setup are described in the Supplemental Material [20]. Electrons were excited into initially unoccupied states above  $E_F$  with 100-fs MIR laser pulses of tunable photon energy ( $h\nu_1=0.25\text{--}0.37$  eV). The transient population was subsequently probed by photoemission of these electrons using ultraviolet (UV) laser pulses ( $h\nu_2=5.16$  eV, 80 fs) [Fig. 1 (a)]. Both  $p$ -polarized beams were focused on the sample into a spot with a diameter of  $\sim 100$   $\mu\text{m}$  using a non-collinear geometry. The experiments were carried out in a  $\mu$ -metal shielded UHV chamber at a base pressure of  $4 \times 10^{-11}$  mbar. Photoelectrons were collected along the high symmetry line  $\bar{\Gamma}$ - $\bar{K}$  by a hemispherical analyzer (Specs Phoibos 150) with a display-type detector. A single crystal of  $p$ -doped  $\text{Sb}_2\text{Te}_3$  was cleaved *in situ* by the Scotch tape method at a pressure of  $3 \times 10^{-10}$  mbar followed by a rapid recovery back to the base pressure within a minute. The Dirac point (DP) of the sample was located  $\sim 150$  meV above  $E_F$ . During the measurements the sample temperature was maintained at 300 K or 80 K.

We start by discussing the optical excitation process into the unoccupied TSS by means of Figures 1 (b) and (c), which show angle-resolved 2PPE spectra of  $\text{Sb}_2\text{Te}_3$  using a pump photon energy  $h\nu_1$  of 0.37 eV at 300 K and 80 K, respectively. To avoid interfering 2PPE signals from the image-potential states, which are excited by the UV pulses and probed by the MIR pulses, a 50 fs delay of the UV probe pulses with respect to the MIR pump pulses has been used. Even at this small delay, a

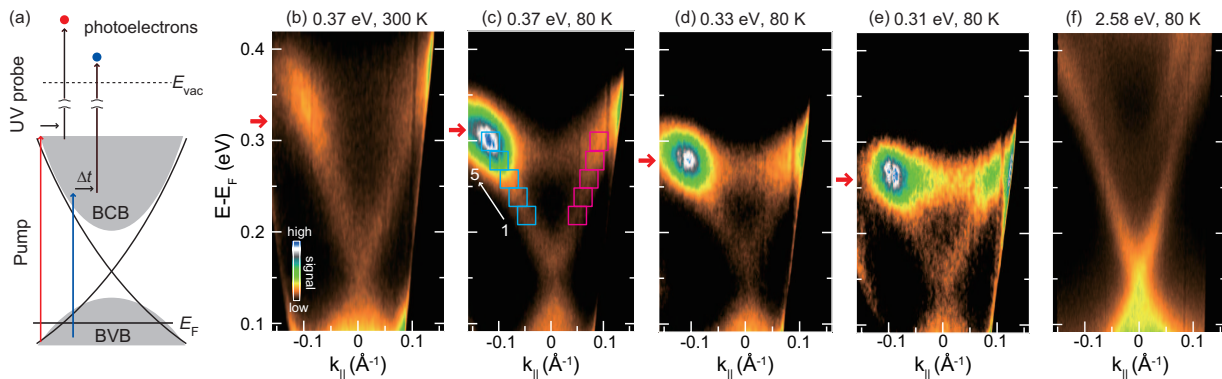


FIG. 1: (Color online) (a) Excitation scheme for the population of the TSS in  $\text{Sb}_2\text{Te}_3$  with MIR pump pulses and subsequent photoemission with ultraviolet probe pulses. (b) and (c) Angle-resolved 2PPE spectra for 0.37 eV pump and 5.16 eV probe pulses 50 fs after MIR excitation at 300 K and 80 K, respectively. Red arrows indicate the energies of maximum population enhancement in the TSS. (d) and (e) show the results acquired at 80 K using 0.33 eV and 0.31 eV pump pulses, respectively. (f) shows a spectrum for 2.58 eV pump pulses for comparison.

considerable population of the TSS can already be observed. It extends only up to 350 meV above  $E_F$  due to the low excitation energy. Curiously, the population of the TSS is pronounced at a specific energy of  $\sim 300$  meV (red arrows). It becomes even more pronounced at 80 K [Fig. 1 (c)], where also a considerable population near the lower edge of bulk conduction band (BCB) at 270 meV can be observed. The specific energy of the population enhancement in the TSS significantly depends on  $h\nu_1$ : it clearly shifts to lower energy with decreasing  $h\nu_1$  even for small changes of  $h\nu_1$  [Fig. 1 (c)-(e)]. The data also clearly shows that the population at  $-k_{||}$  is much more prominent compared to that at  $+k_{||}$ , which represents a strong asymmetric population in  $k$ -space. The population enhancement and its strong asymmetry is not observed for visible pump pulses ( $h\nu_1=2.58$  eV) and the same UV probe pulses [Fig. 1 (f)]. Thus, it turns out that these findings are unique for the optical excitation with MIR pulses.

In order to reveal the origin of the pronounced population at a specific energy, we have investigated its dependence on  $h\nu_1$  by systematic tuning of the MIR pulses. Figure 2 summarizes this dependence for 300 K (red symbols) and 80 K (blue symbols). Obviously, the energy position of the population enhancement is proportional to the excitation energy for both temperatures. This is a clear indication that it is induced by a specific direct optical coupling to the TSS.

In principle, three different optical excitation processes can result in a population of the TSS within this energy range: Firstly, transitions from the bulk valence band (BVB) to the BCB. This process, however, can neither raise the population at a specific energy in the TSS, nor should it show a clear  $h\nu_1$  dependence, because both bands can be coupled over a wide energy range. Secondly, TSS-BCB (BVB-TSS) transitions for which the

initial (intermediate) state is the TSS and the intermediate (initial) state is a bulk state. Thirdly, resonant transitions between the occupied and unoccupied part of the TSS across the DP (TSS-TSS transition).

It can be easily understood that TSS-BCB and BVB-TSS transitions, which are transitions into (from) a continuum of states, should show a linear dependence on  $h\nu_1$  with a slope of unity as depicted by the dashed line in Fig. 2. Obviously, this dependence cannot describe our experimental data. The  $h\nu_1$  dependence of TSS-TSS transitions, on the other hand, is given by the dispersion of the TSS. The population enhancement for this process appears at those intermediate state energies for

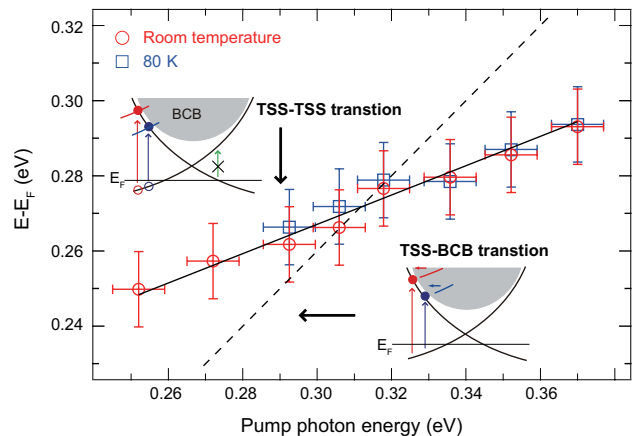


FIG. 2: (Color online) Energy position of the pronounced 2PPE signal created in the TSS as a function of the MIR photon energy acquired at 300 K (red circle) and 80 K (blue circle), respectively. The solid and the dashed line show the simulated energy dependence for TSS-TSS transitions and TSS-BCB transitions (see text for details).

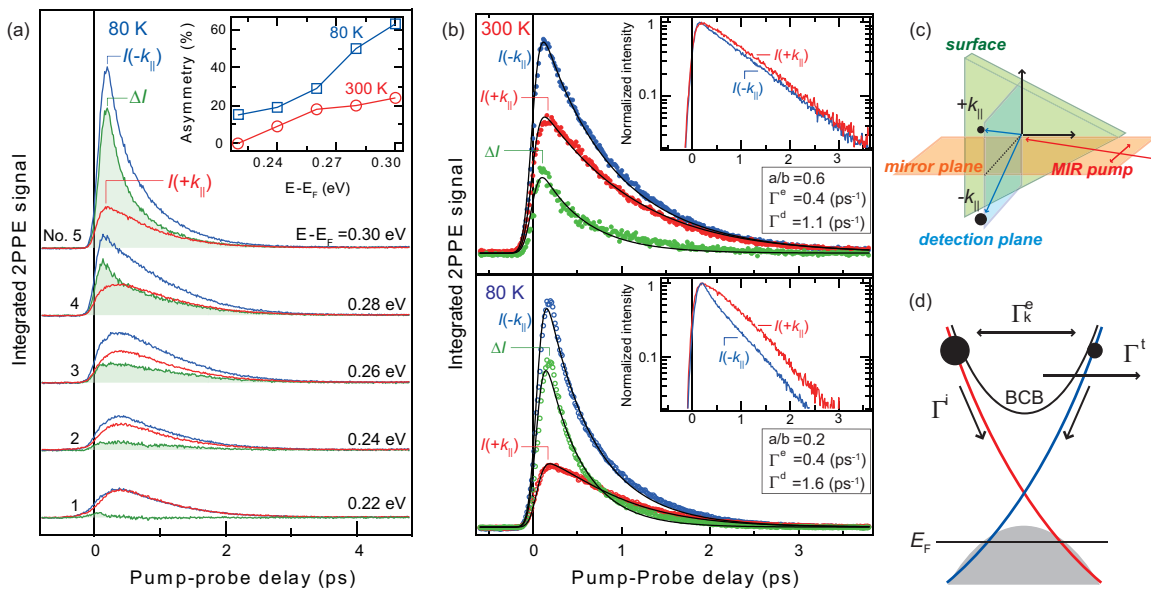


FIG. 3: (Color online) (a) Time-evolutions of the 2PPE signals  $I_{+k}$  (red),  $I_{-k}$  (blue) and their difference  $\Delta I = I_{-k} - I_{+k}$  (green) for different energies at 80 K.  $I_{\pm k}$  is respectively obtained by integrating the 2PPE signal within the windows shown in Fig. 1 (c). The inset depicts the maximum of  $A = \Delta I / (I_{+k} + I_{-k})$  as a function of the energy. (b) Representative line profiles from (a) at the direct excitation energy at 300 K (top) and 80 K (bottom). Solid lines indicate the fitting results of the rate equation model [see the main text]. The fitting parameters are indicated in the figure. The inset shows logarithmic plots of the normalized  $I_{\pm k}$ . (c) Experimental geometry where a mirror plane of the surface coincides with the plane of incidence (red square) perpendicular to the detection plane of photoelectrons (blue square). The triangle depicts the  $C_{3v}$  surface symmetry. (d) Energy and momentum scheme for the decay of the asymmetric population due to elastic scattering within the TSS ( $\Gamma_k^e$ ), inelastic scattering ( $\Gamma^i$ ) and transport ( $\Gamma^t$ ).

which the energy difference between the initial state in the occupied part of the TSS and the intermediate state in the unoccupied part of the TSS just matches  $\hbar\nu_1$ . For the simulation of this process, we have used data on the dispersion of the occupied part of the TSS in  $\text{Sb}_2\text{Te}_3$  from Ref. [24] and for the unoccupied part from Ref. [18]. The almost linear dispersion of the TSS results in a simple linear dependence on  $\hbar\nu_1$  as depicted by the solid line in Fig. 2 which can excellently reproduce our experimental results. The simulation furthermore predicts that TSS-TSS transitions are not possible for  $\hbar\nu_1$  below 0.27 eV at which the initial state becomes unoccupied. This is also in very good agreement with our finding that the population in the TSS strongly drops for  $\hbar\nu_1$  below 0.25 eV. It is therefore concluded that MIR pulses are able to drive a direct optical transition from the lower into the upper part of the TSS.

One may wonder why such a transition between states of opposite chiral spin textures across the DP are allowed, since spin-flip excitations are forbidden in the dipole approximation. However, if spin-orbit coupling plays an important role, the TSS cannot be fully spin polarized and this selection rule is softened. In fact, a spin polarization of below 80% has been discussed for the TSS in different 3D TIs [25–28]. In addition, a hybridization with bulk states [29] possibly results in a further reduc-

tion of the spin polarization [24].

We now turn to the asymmetry of the excited population which is only observed for direct excitation with MIR pulses. Its time and energy evolution is shown in Fig. 3 (a), where we have plotted the transient 2PPE intensity at  $\pm k$  as well as its difference for different energies as depicted by the five integration windows in Fig. 1 (c). For all energies, the 2PPE intensity shows a fast rise within the time resolution of  $\approx 200$  fs and a subsequent decay within a few picoseconds. This is in strong contrast to the delayed dynamics observed for 800-nm, or visible excitation [12–18], and corroborates the direct excitation process of the TSS. The asymmetry  $A = \Delta I / (I_{-k} + I_{+k})$  reaches up to 60% at the direct excitation energy and strongly drops for energies below. We observe such large asymmetry along  $\Gamma$ - $\bar{K}$  for  $p$ -polarized MIR pulses but almost no contrast between opposite helicities of circular polarized light [20]. This is surprising for our geometry where a mirror plane of the surface coincides with the plane of incidence [Fig. 3 (c)]. It indicates that the three-fold symmetry of the surface might be broken. Possible reasons for such symmetry break can be oriented step edges on the cleaved surface which superimpose a one-fold symmetry, a distortion of the first quintuple layer with respect to the underlying bulk, or a non-perfect azimuthal orientation of the sample, which was, however,

oriented within better than  $5^\circ$  [20]. Independent of its actual origin, a  $k$ -space asymmetry of the population in the intermediate state directly reflects a photocurrent parallel to the surface [30]. This is verified by the observation of a distinct dynamics of the 2PPE signal for opposite momenta at the direct excitation energy [Fig. 3 (b)], which is most clearly seen in the logarithmic plot of the normalized intensities [inset of Fig. 3 (b)]. The decay at  $-k$  is initially faster as compared to the decay at  $+k$  due to momentum scattering which progressively equalizes the asymmetry. On a longer timescale, both signals decay with a common time constant due to inelastic decay. In accordance with the intensity contrast, the difference of the decay dynamics is more pronounced at 80 K as compared to 300 K [Fig. 3 (b)]. These findings unambiguously reveal that the novel direct optical excitation generates a transient photocurrent in the TSS.

To analyze the dynamics of the photocurrent in more detail, we use a rate-equation model which is depicted in Fig. 3 (d). It describes the populations  $n_{+k}$  and  $n_{-k}$  at the direct excitation energy where no indirect filling from higher-lying states can occur:

$$\begin{aligned}\frac{dn_{+}}{dt} &= a\delta(t) - \Gamma_k^e n_{+} + \Gamma_k^e n_{-} - \Gamma^d n_{+} \\ \frac{dn_{-}}{dt} &= b\delta(t) - \Gamma_k^e n_{-} + \Gamma_k^e n_{+} - \Gamma^d n_{-}\end{aligned}$$

Here,  $\delta(t)$  is the temporal intensity profile of the Gaussian shaped MIR laser pulse, and  $a$  and  $b$  indicate the different excitation probabilities of electrons at  $+k_{\parallel}$  and  $-k_{\parallel}$ , respectively. In our model,  $n_{+k}$  and  $n_{-k}$  exchange electrons with an elastic scattering rate ( $\Gamma_k^e$ ) which includes momentum and spin scattering. Both mechanisms are closely related to each other due to the spin structure of the Dirac cone but might only be disentangled by a direct observation of the spin dynamics. Both populations mutually decay with an effective total population decay rate ( $\Gamma^d$ ). Beside the inelastic decay into lower-lying states ( $\Gamma^i$ ),  $\Gamma^d$  includes interband scattering into the BCB with subsequent bulk transport ( $\Gamma^t$ ), because the direct excitation energy is close to the BCB bottom [18].  $\Gamma^d$  is thus defined as  $\Gamma^d = \Gamma^i + \Gamma^t$ .

By assuming that  $I_{\pm k} \propto n_{\pm k}$ , the difference  $\Delta I = I_{+k} - I_{-k}$  directly reflects the photocurrent in the TSS. With the two rate equations above, it is described by:

$$\frac{d\Delta I}{dt} = (b - a)\delta(t) - (2\Gamma_k^e + \Gamma^d)\Delta I$$

The photocurrent thus decays exponentially with a time constant  $\tau^c = 1/(2\Gamma_k^e + \Gamma^d)$  which is governed by both elastic momentum scattering and total population decay. Best fits for this model of the experimental data  $I_{\pm k}$  and  $\Delta I$  are shown as solid lines in Fig. 3 (b). Clearly, even this simple model can reproduce the experimental data for both temperatures very well.  $\Gamma^d$  is for both temperatures much larger compared to  $\Gamma_k^e$  through  $\Gamma^i$ ,

because electron-hole pair creation in the incompletely filled VB is an important inelastic decay channel for  $p$ -doped samples.  $\tau^c = 0.42$  (0.52) ps at 80 (300) K is therefore governed by the overall population decay of the TSS. The increase of  $\Gamma^d$  at 80 K as compared to 300 K can be explained by an enhancement of  $\Gamma^t$ , which shows quantitatively good agreement with our recent work on  $\text{Sb}_2\text{Te}_2\text{Se}$  [18]. In contrast,  $\Gamma_k^e$  shows no significant change with temperature although the Debye temperature of  $\text{Sb}_2\text{Te}_3$  ( $\theta_D = 162$  K [31]) is well between the two investigated temperatures. We thus conclude that phonon scattering plays only a minor role for  $\Gamma_k^e$  and surface imperfections like steps or defects are most likely the main factors for elastic scattering. Beyond defect scattering, interband scattering into and from the BCB, where backscattering is allowed, might also be possible due to the large wavefunction overlap of the TSS with the BCB. Both scattering processes effectively increase  $\Gamma_k^e$  which ultimately limits the lifetime of the photocurrent even if  $\Gamma^d$  can be suppressed. Indeed,  $\Gamma_k^e$  becomes the main factor for the transport properties under static electric fields if the sample is close to charge neutrality. In any case, the decay time  $\tau_k^e = 1/\Gamma_k^e = 2.5$  ps is quite long, if for example, compared to dephasing times of quantum beats between image potential states on well prepared noble metal surfaces [33–35]. Such a slow randomization of momentum holds a general advantage also for application under static conditions. If the main process of  $\Gamma_k^e$  is in fact defect scattering, high-quality thin film samples might further increase the mobility of electrons in the TSS.

In conclusion, we have shown that MIR pulses generate a novel optical coupling between the occupied and the unoccupied part of the TSS across the DP, which permits an ultrafast direct excitation of the TSS. Our data unambiguously reveal that this novel direct excitation generates an unbalanced transient electron population in  $k$ -space, which directly mirrors a photoexcited electric current in the TSS. Even if the polarization dependence of the current generation is not fully understood yet, our discovery opens a pathway for a coherent optical control of the TSS via an ultrafast optical excitation with MIR pulses.

We thank H. Bentmann and F. Reinert for providing us  $\text{Sb}_2\text{Te}_3$  samples and gratefully acknowledge funding by the Deutsche Forschungsgemeinschaft through SPP1666 and GU495/2. K. K. acknowledges support from JSPS Postdoctoral Fellowship for Research Abroad.

- 
- [1] M. Z. Hasan and C. L. Kane, Rev. Mod. Phys. **82**, 3045 (2010).
  - [2] Y. Xia, D. Qian, D. Hsieh, L. Wray, A. Pal, H. Lin, A. Bansil, D. Grauer, Y. S. Hor, R. J. Cava, M. Z. Hasan, Nature Phys. **5**, 398 (2009).

- [3] Y. L. Chen, J. G. Analytis, J. H. Chu, Z. K. Liu, S. K. Mo, X. L. Qi, H. J. Zhang, D. H. Lu, X. Dai, Z. Fang, S. C. Zhang, I. R. Fisher, Z. Hussain and Z. X. Shen, *Science* **325**, 178 (2009).
- [4] C. Jozwiak, C. H. Park, K. Gotlieb, C. Hwang, D. H. Lee, S. G. Louie, J. D. Denlinger, C. R. Rotundu, R. J. Birgeneau, Z. Hussain and A. Lanzara, *Nature Phys.* **9**, 293 (2013).
- [5] J. W. McIver, D. Hsieh, H. Steinberg, P. Jarillo-Herrero and N. Gedik, *Nature Nanotech.* **7**, 96 (2012).
- [6] P. Olbrich, L. E. Golub, T. Herrmann, S. N. Danilov, H. Plank, V. V. Belkov, G. Mussler, C. Weyrich, C. M. Schneider, J. Kampmeier, D. Grutzmacher, L. Plucinski, M. Eschbach, and S. D. Ganichev, *Phys. Rev. Lett.* **113**, 096601 (2014).
- [7] Christoph Kastl, Christoph Kurnetzky, Helmut Karl, and Alexander W. Holleitner, *Nature Comm.* **6**, 6617 (2015).
- [8] H. Wang, H. Steinberg, P. Jarillo-Herrero, and N. Gedik, *Science* **25**, 453 (2013).
- [9] J. Qi, X. Chen, W. Yu, P. Cadden-Zimansky, D. Smirnov, N. H. Tolk, I. Miotkowski, H. Cao, Y. P. Chen, Y. Wu, S. Qiao and Z. Jiang, *Appl. Phys. Lett.* **97**, 182102 (2010).
- [10] D. Hsieh, F. Mahmood, J. W. McIver, D. R. Gardner, Y. S. Lee, and N. Gedik, *Phys. Rev. Lett.* **107**, 077401 (2011).
- [11] *"Dynamics at Solid State Surfaces and Interfaces: Volume 1 - Current Developments"*, edited by U. Bovensiepen, H. Petek, and M. Wolf (Wiley-VCH, Berlin, 2010).
- [12] J. A. Sobota, S. Yang, J. G. Analytis, Y. L. Chen, I. R. Fisher, P. S. Kirchmann, and Z. X. Shen, *Phys. Rev. Lett.* **108**, 117403 (2012).
- [13] Y. H. Wang, D. Hsieh, E. J. Sie, H. Steinberg, D. R. Gardner, Y. S. Lee, P. Jarillo-Herrero, and N. Gedik, *Phys. Rev. Lett.* **109**, 127401 (2012).
- [14] A. Crepaldi, B. Ressel, F. Cilento, M. Zacchigna, C. Grazioli, H. Berger, Ph. Bugnon, K. Kern, M. Grioni, and F. Parmigiani, *Phys. Rev. B* **86**, 205133 (2012).
- [15] M. Hajlaoui, E. Papalazarou, J. Mauchain, G. Lantz, N. Moisan, D. Boschetto, Z. Jiang, I. Miotkowski, Y. P. Chen, A. Taleb-Ibrahimi, L. Perfetti, and M. Marsi, *Nano Lett.* **12**, 3532 (2012).
- [16] D. Niesner, S. Otto, V. Hermann, T. Fauster, T. V. Menshchikova, S. V. Eremeev, Z. S. Aliev, I. R. Amiraslanov, M. B. Babanly, P. M. Echenique, and E. V. Chulkov, *Phys. Rev. B* **89**, 081404 (2014).
- [17] J. A. Sobota, S. L. Yang, A. F. Kemper, J. J. Lee, F. T. Schmitt, W. Li, R. G. Moore, J. G. Analytis, I. R. Fisher, P. S. Kirchmann, T. P. Devereaux, and Z. X. Shen, *Phys. Rev. Lett.* **111**, 136802 (2013).
- [18] J. Reimann, J. Gdde, K. Kuroda, E. V. Chulkov and U. Hfer, *Phys. Rev. B* **90**, 081106 (2014).
- [19] S. Zhu, Y. Ishida, K. Kuroda, K. Sumida, M. Ye, J. Wang, H. Pan, M. Taniguchi, S. Qiao, S. Shin, A. Kimura, *Sci. Rep.* **5**, 13213 (2015).
- [20] See Supplemental Material at [<http://...>], which includes Refs. [6, 21–23].
- [21] M. M. Glazov, S. D. Ganichev, *Phys. Rep.* **535**, 101 (2014).
- [22] A. Junck, G. Refael, and F. von Oppen, *Phys. Rev. B* **88**, 075144 (2013).
- [23] Y. Onishi, Z. Ren, M. Novak, K. Segawa, Y. Ando, and K. Tanaka, *arXiv:1403.2492* (2014).
- [24] C. Pauly, G. Bihlmayer, M. Liebmann, M. Grob, A. Georgi, D. Subramaniam, M. R. Scholz, J. Sanchez-Barriga, A. Varykhalov, S. Blugel, O. Rader, and M. Morgenstern, *Phys. Rev. B* **86**, 235106 (2012).
- [25] O. V. Yazyev, J. E. Moore, and S. G. Louie, *Phys. Rev. Lett.* **105**, 266806 (2010).
- [26] Z.-H. Pan, E. Vescovo, A. V. Fedorov, D. Gardner, Y. S. Lee, S. Chu, G. D. Gu, and T. Valla, *Phys. Rev. Lett.* **106**, 257004 (2011).
- [27] S. Souma, K. Kosaka, T. Sato, M. Komatsu, A. Takayama, T. Takahashi, M. Kriener, K. Segawa, and Y. Ando, *Phys. Rev. Lett.* **106**, 216803 (2011).
- [28] K. Miyamoto, A. Kimura, T. Okuda, H. Miyahara, K. Kuroda, H. Namatame, M. Taniguchi, S. V. Eremeev, T. V. Menshchikova, E. V. Chulkov, K. A. Kokh, and O. E. Tereshchenko, *Phys. Rev. Lett.* **109**, 166802 (2012).
- [29] C. Seibel, H. Bentmann, J. Braun, J. Minar, H. Maass, K. Sakamoto, M. Arita, K. Shimada, H. Ebert, and F. Reinert, *Phys. Rev. Lett.* **114**, 066802 (2015).
- [30] J. Gdde, M. Rohleder, T. Meier, S. W. Koch, U. Hfer, *Science* **318**, 1287 (2007).
- [31] J. S. Dyck, W. Chen, C. Uher, C. Drasar, P. Lostak, *Phys. Rev. B* **66**, 125206 (2002).
- [32] S. Kim, S. Yoshizawa, Y. Ishida, K. Eto, K. Segawa, Y. Ando, S. Shin, and F. Komori, *Phys. Rev. Lett.* **112**, 136802 (2014).
- [33] U. Hfer, I. L. Shumay, C. Reu, U. Thomann, W. Wal-lauer, and T. Fauster, *Science* **277**, 1480 (1997).
- [34] C. Reu, I. L. Shumay, U. Thomann, M. Kutschera, M. Weinelt, T. Fauster, and U. Hfer, *Phys. Rev. Lett.* **82**, 153 (1999).
- [35] M. Marks, C. H. Schwalb, K. Schubert, J. Gdde, and U. Hfer, *Phys. Rev. B* **84**, 245402 (2011).